

A quest for frustration driven distortion in $Y_2Mo_2O_7$

Eva Sagi, Oren Ofer, and Amit Keren

Physics Department, Technion, Israel Institute of Technology, Haifa 32000, Israel

Jason S. Gardner

*Physics Department, Brookhaven National Laboratory, Upton,
New York 11973-5000 & NIST Center for Neutron Research,
National Institute of Standards and Technology, Gaithersburg, Maryland 20899-8562*

(Date textdate)

We investigated the nature of the freezing in the geometrically frustrated Heisenberg spin-glass $Y_2Mo_2O_7$ by measuring the temperature dependence of the static internal magnetic field distribution above the spin-glass temperature, T_g , using the μ SR technique. The evolution of the field distribution cannot be explained by changes in the spin susceptibility alone and suggests a lattice deformation. This possibility is addressed by numerical simulations of the Heisenberg Hamiltonian with magneto-elastic coupling at $T > 0$.

PACS numbers: 75.50.Lk, 75.10.Nr

A geometrically frustrated magnet is one whose symmetry precludes every pairwise interaction in the system being satisfied simultaneously. Such systems can have “macroscopic” degenerate ground states, which prevents the system from settling into a unique state as the temperature is lowered. In this situation, small perturbations to the Hamiltonian can have a dramatic effect, selecting one ground state over another. It has been suggested that the ground state degeneracy of the Heisenberg antiferromagnet on the pyrochlore lattice, a lattice of corner-sharing tetrahedra, can be lifted by a magneto-elastic coupling^{1,2,3,4,5,6}. Such a coupling allows the lattice to distort in order to relieve the magnetic frustration, concomitantly lowering the total system energy. Since the 3D corner-sharing tetrahedra lattice is susceptible to distortion under arbitrarily small magneto-elastic coupling, it is at the centre of an ongoing quest to observe this phenomena. Several materials show a lot of promise in this respect, including several Cr^{3+} spinels and several $A_2B_2O_7$ pyrochlores^{5,6,7}.

One promising, but puzzling, candidate is $Y_2Mo_2O_7$ [YMO]. YMO is a narrow-band semiconductor with a Curie-Weiss temperature of ~ 200 K and a spin-glass transition at 22.5 K⁸. The glassiness of the system implies some kind of disorder in the exchange integral, whose origin might be a deformed lattice. Indeed, Booth *et al.*⁹ showed, using the X-ray-absorption fine-structure technique, that the Mo tetrahedra are in fact distorted at the local level by about 5%. This relatively large amount of bond disorder is not seen by the usual diffraction techniques (X-rays or neutrons), indicating that the average bulk structure is almost the perfect oxide pyrochlore lattice⁸. Further evidence of disorder was revealed by ^{89}Y NMR⁵, where regularly spaced peaks implied the existence of many non-equivalent ^{89}Y sites. These features were attributed to distortions in the Mo-sublattice. However, the NMR data were limited to nitrogen temperatures due to limitations on the maximum RF power available in Helium atmosphere, and the decrease of signal in-

tensity with decreasing temperature due to the abnormal increase of the line width. To gain a better understanding of the freezing process in YMO, and to determine whether a lattice deformation is active close to T_g , we performed a study similar to the NMR one and with the same sample, using muon spin rotation and relaxation techniques. In this letter we present these μ SR results and attempt to reconcile them (and the NMR) with the existing diffraction data through numerical simulations.

Transverse [TF] and longitudinal field [LF] μ SR measurements were performed on the GPS spectrometer at the Paul Scherrer Institute, Switzerland. The measurements were carried out with the muon spin tilted by 50° relative to the direction of the applied magnetic field of 6 kG, and positron data were accumulated in both the forward-backward (longitudinal) and the up-down (transverse) directions simultaneously. This allows us to determine both transverse and longitudinal muon spin relaxation rates. In Fig. 1 we show the LF [panel (a)] and the TF data [panels (b) and (c)] at two temperatures. Both TF and LF relaxation rates increase with decreasing temperature; however, at 23.2 K the transverse asymmetry is zero after 0.6 μ sec while the longitudinal asymmetry is still finite at much longer times. This means that close to T_g the TF relaxation is larger than the LF one and most of the in-plane depolarization is from static field inhomogeneities.

We found that the μ SR LF asymmetry is best described by the root exponential

$$A_{LF}(t) = A_0 \exp(-(R_{LF}t)^{\frac{1}{2}}) + B_g \quad (1)$$

where the parameters A_0 are set by taking into account the tilt of the muon spin relative to the longitudinal magnetic field, R_{LF} is the longitudinal relaxation rate, and t is time. Similarly, the TF asymmetry is best fitted by a root exponential superimposed on a cosine oscillation with a transverse relaxation rate R_{TF} :

$$A_{TF}(t) = A_0 \exp(-(R_{TF}t)^{\frac{1}{2}}) \cos(\omega t + \phi) + B_g. \quad (2)$$

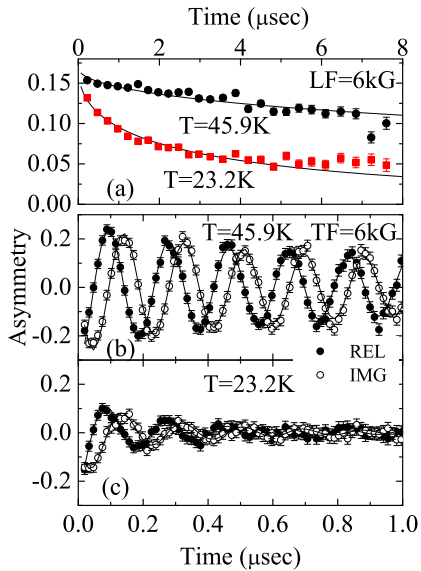


FIG. 1: (a) Longitudinal field asymmetries for $T = 23.2$ K and $T = 45.2$ K; (b) and (c) real and imaginary transverse field asymmetries for $T = 45.2$ K and $T = 23.2$ K respectively. The solid lines are fits to Eqs 1 and 2.

A_0 , the muon rotational frequency ($\omega = \gamma_\mu H_{TF}$), and the background (B_g) are common for all the TF data sets. Since the TF relaxation is a result of both static field inhomogeneity and dynamically fluctuating fields, and the LF relaxation stems from dynamic fluctuations only, we can extract the rates of the two processes. The static field distribution alone will lead to a polarization function of the form

$$P_{static}(t) = P_0 \exp(-(\Delta t)^{1/2}) \cos(\omega t) \quad (3)$$

where $\Delta = [R_{TF}^{1/2} - R_{LF}^{1/2}]^2$ assuming isotropic fluctuations.

In Fig. 2 we plot R_{TF} , R_{LF} , and Δ on a log scale vs. T on the upper part of the abscissa. As the temperature is lowered the difference between R_{TF} and R_{LF} increases. In addition Δ grows exponentially on this semi-log plot upon cooling. In the inset of Fig. 2 we present Δ for various fields at $T = 22.5$ K. One can clearly see that Δ grows with increasing field, and therefore we performed the experiment in the highest field available.

The static relaxation rate Δ is related to lattice deformation via the muon coupling to its neighboring spins and the system's susceptibility. To demonstrate this relation let's assume for simplicity that the muon is coupled only to one electronic spin \mathbf{S} (extension to multiple couplings is trivial). In this case the magnetic field experienced by the muon is a sum of the external field \mathbf{H}_{TF} and the field from the neighboring electron $\mathbf{H}_{int} = g\mu_B \mathbf{A}\mathbf{S}$ where g is the g factor, and μ_B is the Bohr magneton. Here $\mathbf{A} = \mathbf{A}(\mathbf{r})$ is the coupling between the muon and electron spin, which we assume depends on the distance between them, although at present the origin of this cou-

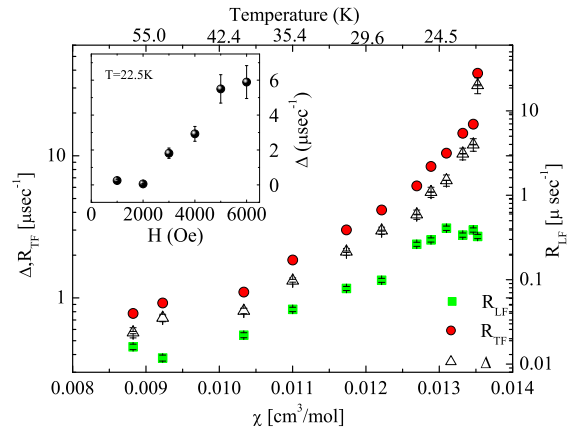


FIG. 2: A plot of the static (Δ), longitudinal (R_{LF}) and transverse (R_{TF}) relaxations rates, on a log scale, versus susceptibility and temperature. In the inset we present Δ versus magnetic field at a constant temperature of 22.5 K.

pling is unknown. In a mean field approximation, $\mathbf{S} \rightarrow \langle \mathbf{S} \rangle = \chi \mathbf{H}_{TF} / g\mu_B$. Therefore, the muon experiences a magnetic field $\mathbf{B} = (1 + \mathbf{A}\chi) \mathbf{H}_{TF}$. Assuming that the susceptibility and the couplings are isotropic, the time evolution of a muon spin due to static field inhomogeneity is given by:

$$P_{static}(t) = \int P_0 \cos[\gamma_\mu (1 + A\chi) H_{TF} t] \rho(A) dA. \quad (4)$$

From Eqs. (3) and (4) we find that $\rho(A) = f(\delta A / \{2\pi|A|\}) / (2|A|)$ where the effective width of the distribution, δA , is given by $\delta A = |\Delta / (\chi \gamma_\mu H_{TF})|$ and f can be expressed in terms of trigonometric and Fresnel functions¹⁰.

If the ratio between Δ and χ remains constant as the temperature changes, the distribution of couplings $\rho(A)$ is temperature independent. Unlike most magnets, this is not the case for YMO. In Fig. 2 we also present on the lower part of the abscissa the susceptibility measured at 6 kG with the temperature as an implicit parameter. We see that Δ is not proportional to and not even a linear function of χ . We thus conclude that the distribution of coupling constants broadens extremely fast upon cooling below 40 K due to random lattice distortions similar to those seen in the NMR work at higher temperatures⁵.

The local lattice distortions or strains discussed above have been elucidated from magnetic probes (μ SR and NMR) in a finite field. At first sight these contradict previously published diffraction data where no structural deviations from the $Fd\bar{3}m$ space group were observed^{8,11}. More recent neutron powder diffraction results in finite applied fields also reveal no unusual thermal dependence on the oxide pyrochlore structure¹². However, Booth and coworkers did find a 5% distribution in Mo-Mo bond lengths in zero field. This quandary, the apparent con-

flict between the data sets, required revisiting the theory of magneto-elastic deformation of the pyrochlore lattice. We have tried to do this through computer simulations where we posed the questions: (I) Can the computer find a classical ground state with a lower energy than that suggested theoretically? (II) How good are the theoretical approximations? and (III) Since experiments are done at finite temperature, what is the effect of thermal fluctuations on spin and spatial correlations?

The Hamiltonian we simulate is the Heisenberg anti-ferromagnet with a magneto-elastic term as illustrated in the inset of Fig. 3 for a single tetrahedon. The rigid bonds between atomic positions of length R are replaced by springs whose elastic energy is zero when $R = 1$. This Hamiltonian is given by

$$\mathcal{H} = J \sum_{i>j} \mathbf{S}_i \cdot \mathbf{S}_j + J' \sum_{i>j} (\mathbf{S}_i \cdot \mathbf{S}_j) \delta r_{ij} + \frac{k}{2} \sum_{i>j} (\delta r_{ij})^2 \quad (5)$$

where $\delta r_{ij} = |\mathbf{r}_i - \mathbf{r}_j| - 1$ is the change in bond length between spins i and j , J' is the derivative of the exchange J relative to bond length, and k is an elastic constant. The minimum energy of \mathcal{H} per spin is given by

$$\frac{E_{\min}}{N} = -J - \frac{3J'^2}{2k} \quad (6)$$

where N is the number of spins³. This energy is achieved in two $q = 0$ states with long range displacement and spin order dominated by E_g or E_u phonons³. For both phonons there are 4 short bonds of length $1 - J'/k$, and two long bonds of length $\sqrt{1 + 2J'/k + 5(J'/k)^2}$ on each tetrahedra. The difference between the phonons is the arrangement of the short and long bonds on the lattice. In our simulations we use the $q = 0$ state with E_u phonon where all tetrahedra of the same orientation on the lattice distort in the same way.

The simulations are performed on a pyrochlore lattice of 8788 spins. In order to allow for lattice deformation, yet maintain the essence of the spin frustration, the boundary conditions are periodic for the spins and open for the coordinates¹³. The energy minimization was done using a zero temperature Metropolis algorithm which stopped when the change in the simulated system's energy was below the machine precision of eight digits. The value of J' is variable while $J = 1$ and $k = 10$ for all runs. Further details concerning the simulation can be found in Ref.¹⁰. The error bars are determined from an evaluation of the finite size effects: the energy of the $q = 0$ state was calculated using the simulation for different lattice sizes, and seen to converge to the theoretical value as the lattice size goes to infinity. Multiple runs of the simulation with the same initial conditions showed other computational errors to be negligible. It should be noted that despite the fact that Eq. 5 is valid only for small δr_{ij} , in the simulations δr_{ij} can assume any number.

In Fig. 3 we present the energy per spin as obtained for 4 different calculations/simulations: (1) and (2) The

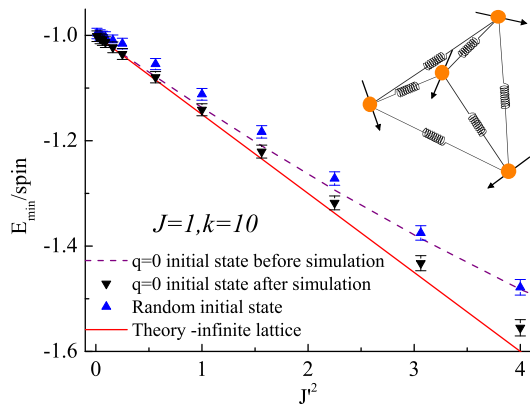


FIG. 3: The minimum energy per spin obtained by the simulation program as described in the text. In the inset we depict a tetrahedral unit of the pyrochlore lattice with its spins connected by springs to enable visualization of the magnetoelastic term.

energy of the $q = 0$ state given by the computer program before and after energy minimization respectively. (3) The final energy of the system after energy minimization of a disordered structure; neither the distortions nor spins entered an ordered state in this case. (4) Eq. 6 adapted to a finite lattice.

At low values of $J'^2/(Jk)$ all four cases agree with each other as expected. However, for high $J'^2/(Jk)$ the simulation depended strongly on the initial simulation state, namely, the ground state manifold for the Hamiltonian is non-ergodic and upon cooling the system can enter one of many metastable states. The discrepancy between cases (1) and (2) stems from large values of δr_{ij} in the simulation that are not consistent with the theory. To summarize the simulations: (I) the computer is unable to find a better state than the $q = 0$ one; (II) the theory is valid in the range $J'^2/k \lesssim 0.1J$; and (III) in this range the disordered states are very close in energy to the $q = 0$ state. This proximity in energy between ordered and disordered states means that low temperatures are needed to isolate the $q = 0$ state. Eq. 6 suggests that this energy scale is set by J'^2/k .

Next we examine the temperature dependence of the correlations by simulating a slow reverse annealing process starting from the $q = 0$ state. In order to follow the displacement and spin correlations we performed computerized magnetic and nuclear neutron scattering, according to Ref.¹⁴, in the 111 direction. The numerical scatterings of several simulation states are shown in the inset of Fig. 4. In panels (a) and (b) we present a reference scattering at zero temperature from the perfect pyrochlore lattice with Heisenberg spins and no magneto-elastic term. In panel (a) we see two peaks which are the trademark of the perfect pyrochlore lattice where the distance between two planes of the same kind (kagome or

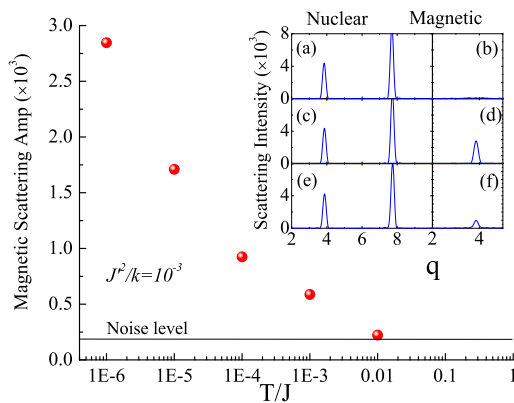


FIG. 4: Nuclear and magnetic computer-simulated neutron scattering in the 111 direction. Inset: (a) Nuclear scattering from a perfect pyrochlore lattice. (b) Magnetic scattering from one of the ground states of the Heisenberg Hamiltonian (without magneto-elastic term) on this lattice. (c)-(f) Nuclear and magnetic scattering from the states obtained by a computer simulation of the Heisenberg Hamiltonian with the magneto-elastic term with $k = 10$ and $J' = 0.1$ (Eq. 5) at different temperatures (note the scale difference). In (c) and (d) $T = 10^{-6}J$ and in (e) and (f) $T = 10^{-4}J$. Main figure: magnetic scattering amplitude as a function of temperature.

triangular) is $2\sqrt{2/3}R$ and between two different planes (kagome-triangular) is $\sqrt{2/3}R$. In panel (b) we see the lack of any spin correlations as expected from the Heisenberg ground states. In panels (c) and (d) we show a similar experiment, but this time at finite temperature ($T = 10^{-6}J$) and with a magneto-elastic term. Under these conditions long range magnetic order is found. However, no effect is detected in the nuclear scattering within our resolution. Panels (e) and (f) are the same as (c) and (d) but at a higher temperature. This reduces both the nuclear and magnetic scattering due to thermal vibrations, but it affects the magnetic scattering to a greater extent. This magnetic scattering amplitude is plotted in Fig. 4 as a function of temperature. Clearly it decreases as the temperature increases and is not measurable at $T > J^2/k$. This is the main result of the simulation.

We use our numerical findings to determine the Hamil-

tonian parameters of YMO in the framework of the magneto-elastic coupling. We compare the theoretical change in bond length, which, to first order, is set by $J'/(kR)$ to the 5% distribution in Mo-Mo distance observed by Booth *et al.*⁹. We also estimate J^2/k by the temperature at which spin freezing is observed in YMO, namely, 22.5 K. From these numbers we conclude that $J' \sim 0.01$ eV/Å and $k \sim 0.1$ eV/Å². These numbers should be considered only as order of magnitudes; if one would take the melting temperature as the point at which the magnetic amplitude drops to $1/e$ of its $T = 0$ value, for example, the estimate of both k and J' would increase by a factor of 10. For comparison in ZnCr_2O_4 , another well studied frustrated Heisenberg spin system with approximately the same spin-spin bond length, $J' = 0.04$ eV/Å¹⁵ and $k = 6.5$ eV/Å²⁷. However, the reason YMO maintains its cubic symmetry at all temperatures is still a puzzle. One possibility emerging from the simulation is the lack of ergodicity; upon cooling the system is stuck in a metastable state and does not relax to its ground state. In this case the bulk cubic symmetry is maintained, but locally the system is under immense strain and slightly distorts from its ideal cubic structure.

To summarize, the width of the internal field distribution Δ , as detected by the μSR , grows upon cooling at a rate which cannot be explained by the increasing susceptibility alone. Therefore, we conclude that the width of the distribution of coupling constants δA also grows upon cooling. We attribute this to temperature dependent lattice distortions. However diffraction techniques show no structural changes and only local probes have revealed a distribution of bond lengths. To address this discrepancy we performed numerical simulations of the Heisenberg Hamiltonian with magneto elastic coupling at finite temperatures. This allowed us to estimate J' and k in Eq. 5 and to suggest that upon cooling the system is trapped in a metastable state.

We are grateful for helpful discussion with Oleg Tchernyshyov and to the machine and instrument groups at Paul Scherrer Institute, Switzerland, whose outstanding efforts have made these experiments possible. Work at Brookhaven National Laboratory is supported by the U.S. Department of Energy under contracts DE-AC02-98CH10886. The authors wish to acknowledge the financial support of NATO through a collaborative linkage grant.

¹ K. Terao, J. Phys. Soc. Jpn. **65**, 1413 (1996).

² Y. Yamashita and K. Ueda, Phys. Rev. Lett. **85**, 4960 (2000).

³ O. Tchernyshyov, R. Moessner, S. L. Sondhi, Phys. Rev. Lett. **88**, 067203 (2002), O. Tchernyshyov, R. Moessner, S. L. Sondhi, Phys. Rev. B **66**, 064403 (2002).

⁴ J. Richter, O. Derzhko, and J. Schulenburg, Phys. Rev. Lett. **93**, 107206 (2004).

⁵ A. Keren and J. S. Gardner, Phys. Rev. Lett. **87**, 177201 (2001).

⁶ S.-H. Lee, C. Broholm, T. H. Kim, W. Ratcliff II, and S.-W. Cheong, Phys. Rev. Lett. **84**, 3718 (2000), P. Carretta, N. Papinutto, C. B. Azzoni, M. C. Mozzati, E. Pavarini, S. Gonthier, and P. Millet, Phys. Rev. B **66**, 094420 (2002).

⁷ A. B. Sushkov, O. Tchernyshyov, W. Ratcliff, S. W. Cheong, and H. D. Drew, cond-mat/0411213.

- ⁸ N. P. Raju, E. Gmelin and R. K. Kremer, Phys. Rev. B. **46**, 5405 (1992).
- ⁹ C. H. Booth, J. S. Gardner, G. H. Kwei, R. H. Heffner, F. Bridges and M. A. Subramanian, Phys. Rev. B **62**, R755 (2000).
- ¹⁰ E. Sagi, M. Sci. Thesis (Technion, 2004).
- ¹¹ K. Blacklock, H. W. White and E. Gurmen, J. Chem. Phys. **73**, 1966 (1980).
- ¹² O. Ofer, J. S. Gardner, A. Keren, to be published (2005).
- ¹³ M. P. Allen and D. J. Tildesley, Computer Simulation of Liquids (Oxford Science Publications, 1987).
- ¹⁴ G. L. Squires, Introduction to the Theory of Thermal Neutron Scattering (Dover Publications, 1997).
- ¹⁵ Y. Kino, B. Luthi and M. E. Mullen, J. Phys. Soc. Jpn. **33**, 687 (1972).